Electronic Supplementary Material

Approaching high oxygen evolution reaction performance by synergetic dual-ion leaching

Hancheng Ma[1], Yao Ding[1] (✉), Jianqi Li[1], Wei Peng[1], and Liqiang Mai[2]

[1] *School of Materials Science and Engineering, Wuhan University of Technology, Wuhan 430070, China*
[2] *State Key Laboratory of Advanced Technology for Materials Synthesis and Processing, Wuhan University of Technology, Wuhan 430070, China*

Supporting information to https://doi.org/10.1007/s12274-024-6812-1

Address correspondence to ydingaf@whut.edu.cn

Computational details

All the calculations are performed in the framework of the density functional theory with the projector augmented plane-wave method, as implemented in the Vienna ab initio simulation package. Spin polarization was also included. The generalzied gradient approximation (GGA) proposed by Perdew, Burke, and Ernzerhof is selected for the exchange-correlation potential. A DFT-D3 scheme of dispersion correction was used to describe the van der Waals (vdW) interactions in molecule adsorption [1]. The cut-off energy for plane wave is set to 450 eV. The energy criterion is set to 1E-05 eV in iterative solution of the Kohn-Sham equation. The electron smearing width of σ = 0.03 eV was employed according to the Gaussian smearing technique.

Ni-Co: Cleaving surface (220) of terminated Ni from a triclinic NiOOH primitive cell and the fractional thickness set to 4.0, then redefined lattice into U=26.62 Å, V=6.06 Å and θ=89.89° to get the NiOOH-base. Cleaving surface (101) of terminated OH from a triclinic CoOOH primitive cell and the fractional thickness set to 1.0, then make 1 × 2 supercells after redefined lattice into a rectangle to get the CoOOH-layer. Then the NiOOH-base loaded the CoOOH-layer with adding 20 Å vacuum thickness to build vacuum slab crystal to construct the heterojunction model Ni-Co with 132 atoms of a maximum mismatch rate of 6.24%.

NiOOH: Cleaving surface (220) of terminated OH from a triclinic NiOOH primitive cell and the fractional thickness set to 4.0, then redefined lattice into U = 26.62 Å, V = 6.06 Å and θ=89.89°, and adding 20 Å vacuum thickness to build vacuum slab crystal to get the slab model NiOOH (220) with 96 atoms.

CoOOH: Cleaving surface (101) of terminated OH from a triclinic CoOOH primitive cell and the fractional thickness set to 2.0, then make a 1 × 2 supercell after redefined lattice into a rectangle, and adding 20 Å vacuum thickness to build vacuum slab crystal to get the slab model CoOOH (101) with 98 atoms.

The Brillouin zone integration is performed using the uniformly distributed scattering of going through the Gamma point to select a 1 × 4 × 1 k-mesh in the Monkhorst-Pack grid to make structure optimization, and we select 2 × 8 × 1 k-mesh to do density of state (DOS) calculations [2]. To simulate the effect of inside a solid, the atoms located in the lower half of the slab were fixed for all calculation models. All the structures are relaxed until the residual forces on the atoms have declined to less than 0.02 eV/Å.

A corrective Hubbard Hamiltonian was added in the calculations to improve the description of the electronic structure of this strongly correlated material. On the basis of previous works, the formalism proposed by Dudarev et al. was used, along with the U-J value of 3.52 eV for the cobalt 3d electrons [3, 4]. A U value of 5.5 eV [5], adapted from the linear response theory calculations of Li and Selloni [6], was utilized for Ni. Where the * refers to the catalytic, and the *one refers to the species that adsorbed on the activity sites. The pathway by which the OER occurs under base condition are generally reported to proceed according to the following step:

$* + H_2O \rightarrow *OH + H+ + e^-$

$*OH \rightarrow *O + H+ + e^-$

$*O + H_2O \rightarrow *OOH + H+ + e^-$

$*OOH \rightarrow * + O_2 + H+ + e^-$

Neglect PV contribution to translation for adsorbed molecules, the free energy was calculated according to the equation of G = E + Hcor − TS = E + Gcor, where E is the energy of every specie obtained from DFT calculations, and S are entropy, while T is 298.15 K. The Hcor and Gcor are the thermal correction to enthalpy and the thermal correction to Gibbs free energy, respectively. These Gcor of *OH、*O、*OOH were taken from the frequency DFT calculation and got value by using Vaspkit.1.4.1 [7]. The Gibbs free energy of the proton-electron pairs related in the PECT progress, whereas the fact that the proton-electron pairs is in equilibrium with gaseous H_2: $G(H+ + e^-) = 1/2\ G(H_2\ (g))$. According to Vaspkit.1.4.1, the internal energy of gas molecular gained from the formula: U(T) = ZPE + ΔU(0-T), the enthalpy of gas molecular gained from the formula: H(T) = U(T) + PV = ZPE + ΔU(0-T) + PV, and the Gibbs free energy of gas molecular gained from the formula: G(T) = H(T) − TS = ZPE + ΔU(0-T) + PV − TS = E_DFT + G_cor'. Where E_DFT is the energy of the free gas molecule obtained from DFT calculations, G_cor' is the thermal correction to Gibbs free energy of the free gas molecule obtained from the frequency DFT calculation and got value by using Vaspkit.1.4.1, with the temperature of 298.15K, the pressure of H_2(g) and H2O(l) were 1 atm and 0.035 bar, and H_2, H_2O input 1 as the value of spin multiplicity. Note that the free energy of a O_2 gas molecule should be calculated by this equation: $G\ (O_2, g) = 2*G\ (H_2O, l) - 2*G\ (H_2, g) + 4.92$ eV.

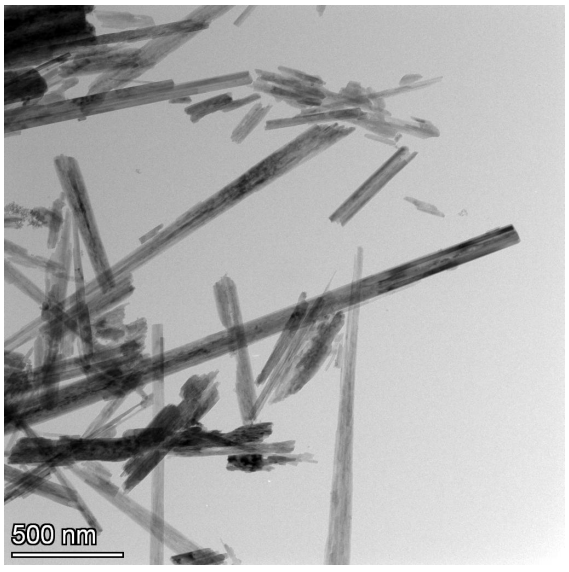

Figure S1 TEM of $NiMoO_4$ showing the morphology of nanorods.

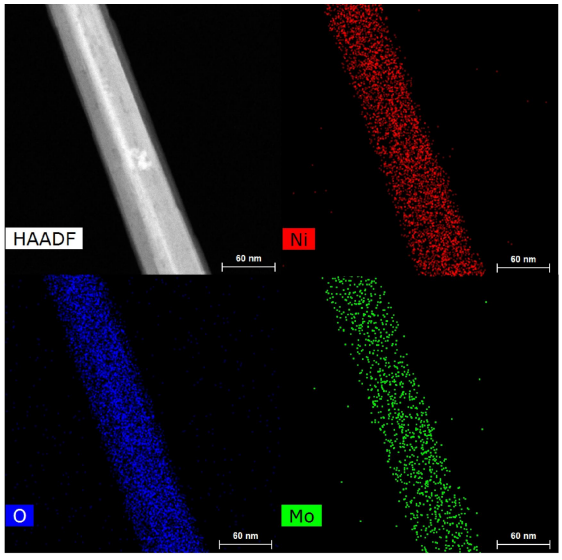

Figure S2 HAADF STEM elements mapping images of $NiMoO_4$.

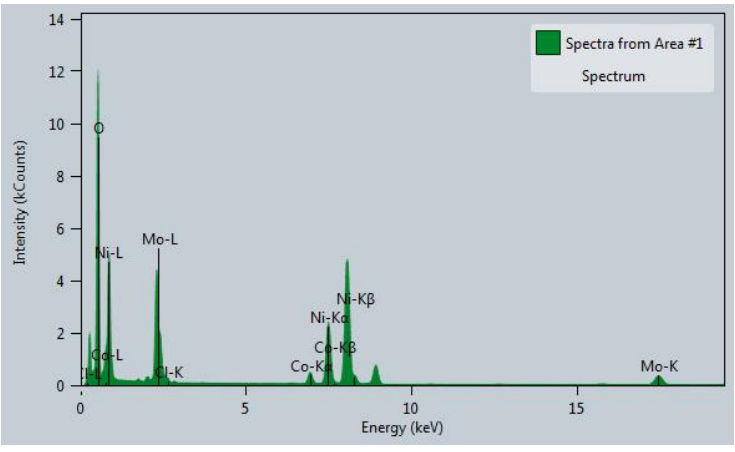

Figure S3 EDX element images of $Co_2(OH)_3Cl$@$NiMoO_4$.

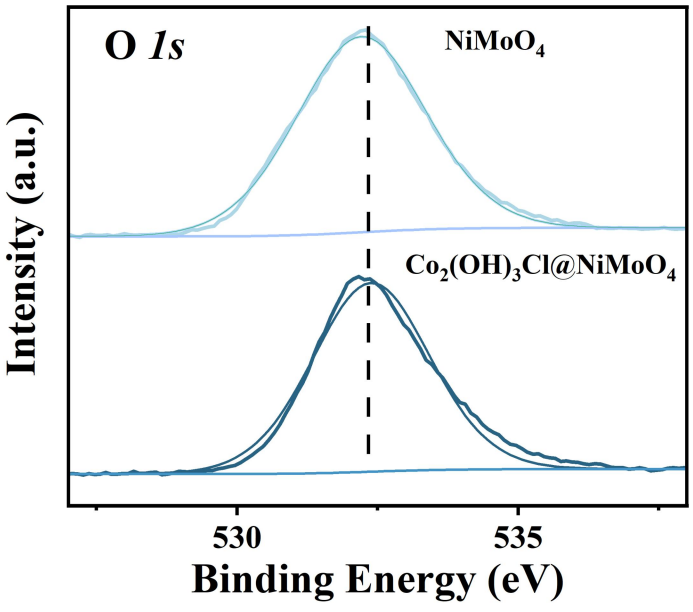

Figure S4 Peaks of O 1s bands in $NiMoO_4$ and $Co_2(OH)_3Cl$@$NiMoO_4$.

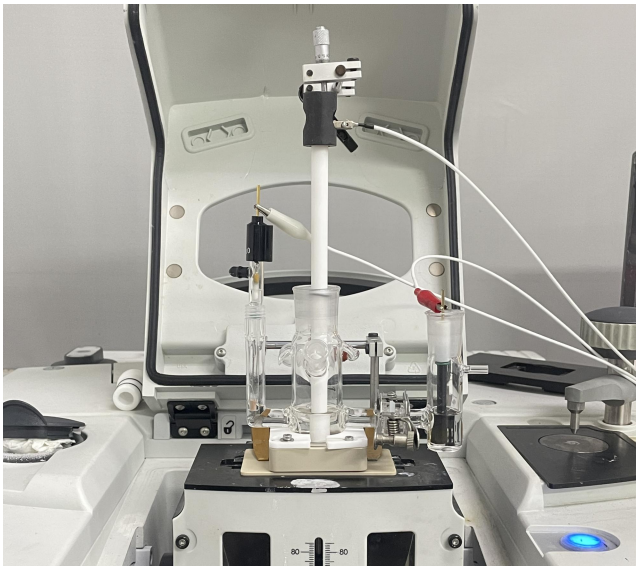

Figure S5 In-situ FT-IR characterization of $Co_2(OH)_3Cl$@$NiMoO_4$.

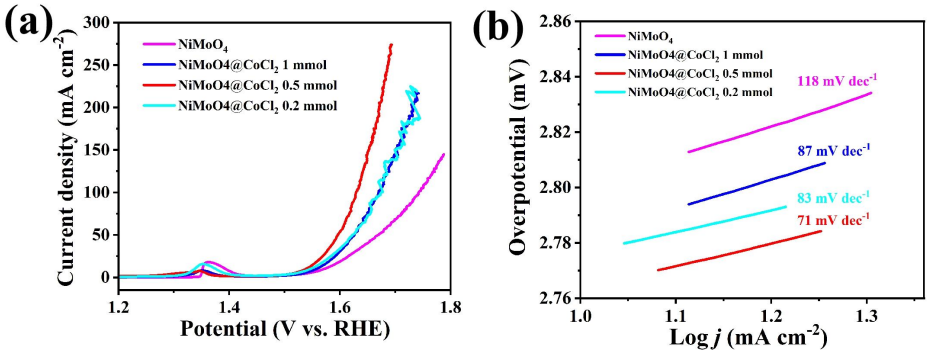

Figure S6 LSV of $NiMoO_4$ for different $CoCl_2$ loading and corresponding Tafel plots.

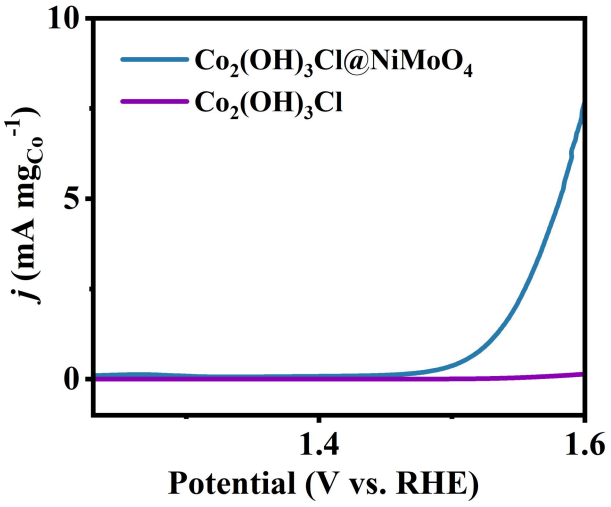

Figure S7 The mass-normalized catalytic activities for $Co_2(OH)_3Cl@NiMoO_4$ and $Co_2(OH)_3Cl$.

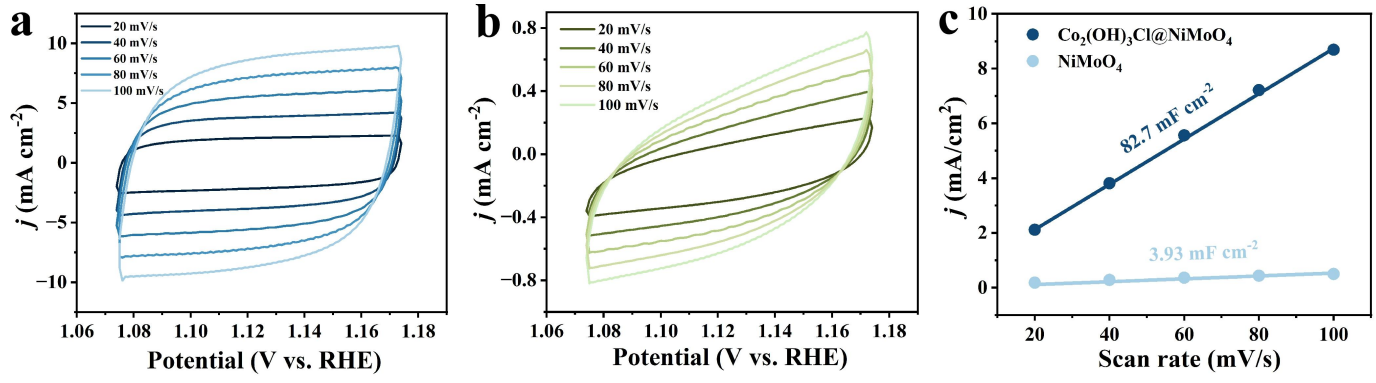

Figure S8 ECSA Performance characterization. Cyclic voltammetry curves at various scan rates for estimation of (a) $Co_2(OH)_3Cl@NiMoO_4$ and (b) $NiMoO_4$. (c) Extraction of the C_{dl} from different electrodes.

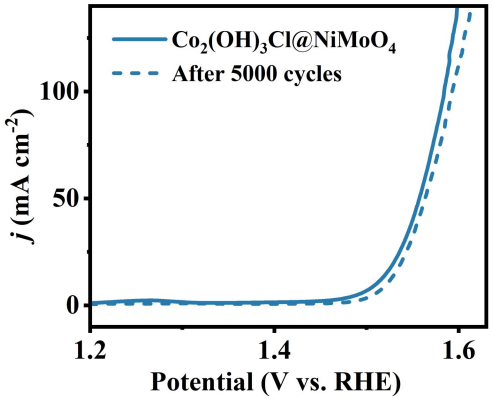

Figure S9 LSV curves of $Co_2(OH)_3Cl@NiMoO_4$ before and after 5000 cycles of accelerated CV test.

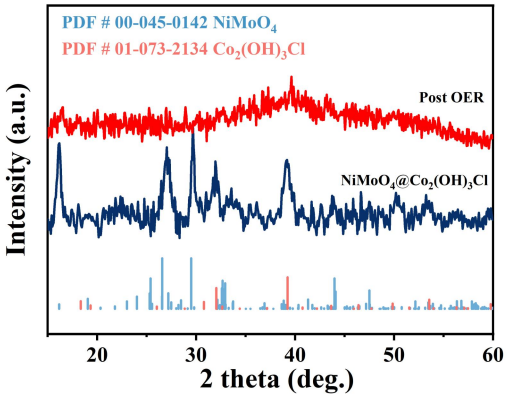

Figure S10 XRD characterization of $Co_2(OH)_3Cl@NiMoO_4$ before and post OER.

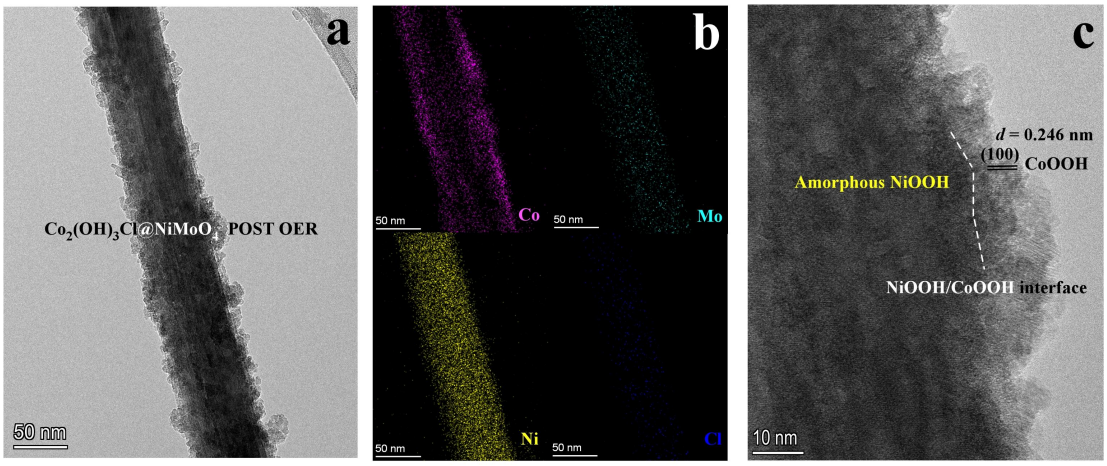

Figure S11 (a) TEM characterization of $Co_2(OH)_3Cl@NiMoO_4$ post OER. (b) HAADF STEM and corresponding elemental mapping images of $Co_2(OH)_3Cl@NiMoO_4$ post OER. (c) High-resolution TEM image of $Co_2(OH)_3Cl@NiMoO_4$ post OER.

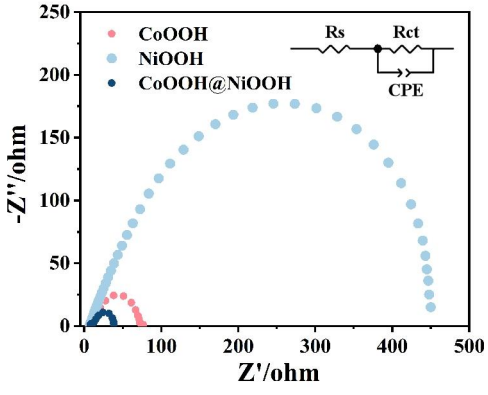

Figure S12 EIS characterization of CoOOH, NiOOH and CoOOH@NiOOH which are obtained by conducting 5000 cycles of accelerated CV test of the $Co_2(OH)_3Cl$, $NiMoO_4$ and $Co_2(OH)_3Cl@NiMoO_4$.

We electrochemically reconstituted $NiMoO_4$, $Co_2(OH)_3Cl@NiMoO_4$ and $Co_2(OH)_3Cl$ and performed EIS tests, respectively. Since the catalysts are reconstituted during the OER process to form NiOOH, CoOOH@NiOOH and CoOOH, respectively, the EIS test results show that the CoOOH@NiOOH with a smaller radius has greatest electron transmission according to form the heterojunction during the electrochemical reconstruction.

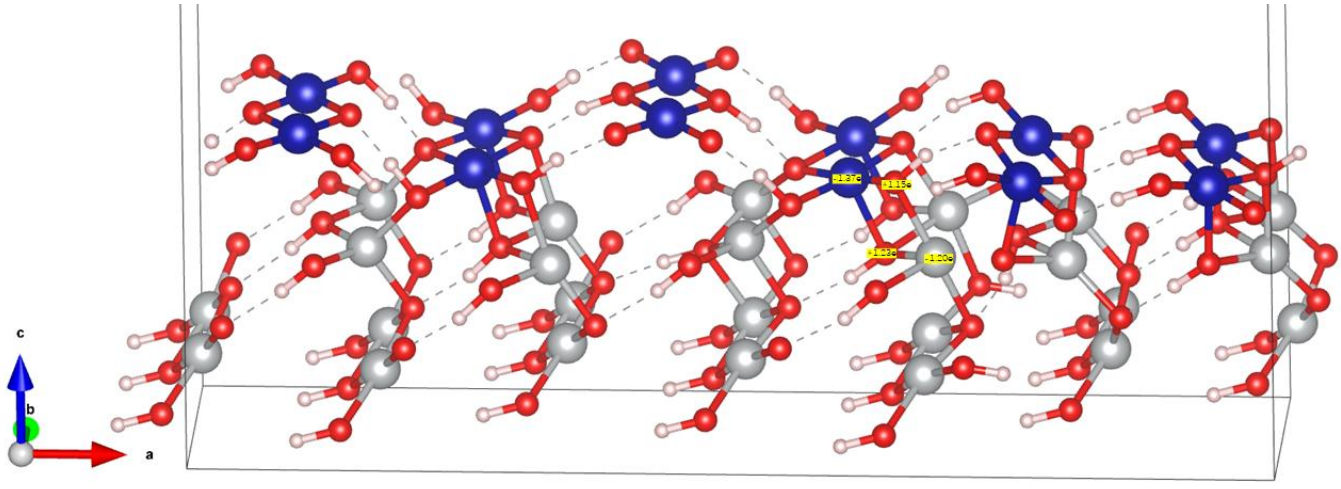

Figure S13 The Barder charge diagram of CoOOH@NiOOH. The direction of electron transfer: from Ni to O and from Co to O.

Table S1 Comparison of OER performance of $NiMoO_4$-based catalysts in 1 M KOH

Catalyst	η (mV)@10 mA cm^{-2}	Tafel slope	Ref.
$NiMoO_4$@$Co_2(OH)_3Cl$	275	62	This work
$NiMoO_4$	340	118	This work
N-$NiMoO_4$/NiS_2	267	74.2	[36]
NCMNT-3	300	68	[37]
$Ni_{0.9}Fe_{0.1}MoO_4$	299	63	[38]
NM-FC2	336	71.8	[39]
c-$Ni_2P_4O_{12}$/c-$NiMoO_x$	370	132	[40]
N-$NiMoO_4$/Ni/CNTs	330	89	[41]

Table S2 ICP testing at different leaching times of $NiMoO_4$@$Co_2(OH)_3Cl$

Time (h)	Mass fraction of Mo (%)	Leaching rate
0 h	26	
4 h	19	0.0875 mg/h
8 h	8	0.1375 mg/h
10 h	6.5	0.0375 mg/h
12 h	6.3	0.005 mg/h

References

[1] Grimme, S.;Antony, J.;Ehrlich, S.; Krieg, H. A consistent and accurate ab initio parametrization of density functional dispersion correction (DFT-D) for the 94 elements H-Pu. *J. Chem. Phys.* **2010**, *132*, 154104.

[2] Chadi, D. J. Special points for Brillouin-zone integrations. *Phys. Rev. B* **1977**, *16*, 1746-1747.

[3] Curutchet, A.;Colinet, P.;Michel, C.;Steinmann, S. N.; Le Bahers, T. Two-sites are better than one: revisiting the OER mechanism on CoOOH by DFT with electrode polarization. *Phys. Chem. Chem. Phys.* **2020**, *22*, 7031-7038.

[4] Bajdich, M.;Garcia-Mota, M.;Vojvodic, A.;Norskov, J. K.; Bell, A. T. Theoretical investigation of the activity of cobalt oxides for the electrochemical oxidation of water. *J. Am. Chem. Soc.* **2013**, *135*, 13521-13530.

[5] Cococcioni, M.; de Gironcoli, S. Linear response approach to the calculation of the effective interaction parameters in the LDA^{+} Umethod. *Phys. Rev. B* **2005**, *71*, 3.

[6] Li, Y.-F.; Selloni, A. Mechanism and Activity of Water Oxidation on Selected Surfaces of Pure and Fe-Doped NiO_x. *ACS Catal.* **2014**, *4*, 1148-1153.

[7] Wang, V.;Xu, N.;Liu, J.-C.;Tang, G.; Geng, W.-T. VASPKIT: A user-friendly interface facilitating high-throughput computing and analysis using VASP code. *Comp. Phys. Commun.* **2021**, *267*, 108033.

[8] Hwang, S. J.;Kim, S. K.;Lee, J. G.;Lee, S. C.;Jang, J. H.;Kim, P.;Lim, T. H.;Sung, Y. E.; Yoo, S. J. Role of electronic perturbation in stability and activity of Pt-based alloy nanocatalysts for oxygen reduction. *J. Am. Chem. Soc.* **2012**, *134*, 19508-19511.

[9] An, L.;Feng, J.;Zhang, Y.;Wang, R.;Liu, H.;Wang, G. C.;Cheng, F.; Xi, P. Epitaxial Heterogeneous Interfaces on N-$NiMoO_4$/NiS_2 Nanowires/Nanosheets to Boost Hydrogen and Oxygen Production for Overall Water Splitting. *Adv. Funct. Mater.* **2018**, *29*, 1805298.

[10] Yin, Z.;Chen, Y.;Zhao, Y.;Li, C.;Zhu, C.; Zhang, X. Hierarchical nanosheet-based $CoMoO_4$-$NiMoO_4$ nanotubes for applications in asymmetric supercapacitors and the oxygen evolution reaction. *J. Mate. Chem. A* **2015**, *3*, 22750-22758.

[11] Chen, J.;Zhao, G.;Chen, Y.;Rui, K.;Mao, H.;Dou, S. X.; Sun, W. Iron-Doped Nickel Molybdate with Enhanced Oxygen Evolution Kinetics. *Chem. Eur. J.* **2018**, *25*, 280-284.

[12] Wang, Z.;Wang, H.;Ji, S.;Wang, X.;Zhou, P.;Huo, S.;Linkov, V.; Wang, R. A High Faraday Efficiency $NiMoO_4$ Nanosheet Array Catalyst by Adjusting the Hydrophilicity for Overall Water Splitting. *Chem.* **2020**, *26*, 12067-12074.

[13] Wang, J.;Hu, J.;Niu, S.;Li, S.;Du, Y.; Xu, P. Crystalline-Amorphous $Ni_2P_4O_{12}$/$NiMoO_x$ Nanoarrays for Alkaline Water Electrolysis: Enhanced Catalytic Activity via In Situ Surface Reconstruction. *Small* **2022**, *18*, e2105972.

[14] Li, G. L.;Qiao, X. Y.;Miao, Y. Y.;Wang, T. Y.; Deng, F. Synergistic Effect of N-$NiMoO_4$/Ni Heterogeneous Interface with Oxygen Vacancies in N-$NiMoO_4$/Ni/CNTs for Superior Overall Water Splitting. *Small* **2023**, *19*, e2207196.